Journal of Materials Chemistry C

RSC Publishing

PAPER

One-step preparation of UV transparent highly ordered mesoporous zirconia thin films†

Cite this: *J. Mater. Chem. C*, 2013, **1**, 1359

Andrés Zelcer*[ab] and Galo J. A. A. Soler-Illia[bc]

Received 2nd October 2012
Accepted 4th December 2012

DOI: 10.1039/c2tc00319h

www.rsc.org/MaterialsC

Highly ordered mesoporous ZrO_2 thin films were prepared by evaporation induced self-assembly. Complexing agents and low pH were simultaneously employed in order to control the hydrolysis–condensation kinetics, permitting to cast films in one step. Many commercially available PPO-based surfactants can be used as templates, yielding different pore sizes. The mesoporosity is well preserved at high temperatures (600 °C) and after exposing the films to extreme alkaline conditions (1 M NaOH, 18 h). The procedure has been used to cast multilayer films, paving the way to mesoporous thin films-based UV photonics.

Introduction

Mesoporous materials, presenting pores between 2 and 50 nm, are promising for multiple applications that benefit from large surface areas: catalysis, sorption, *etc.*[1] When presented as thin films, this family of materials has numerous applications as selective permeation[2] or sorption membranes or in the construction of more complex structures like sensors and photonic materials.[3] In the past few years, an increased amount of work has been dedicated to the development of new methods of preparation and characterization of mesoporous thin films of various chemical compositions (oxides, sulfides, carbon, *etc.*) and pore sizes.[4]

The choice of a mesoporous film as a building block in the design of a device depends on the required physical (refractive index, transparency, conductivity, porosity, crystallinity, *etc.*) and chemical (stability, adsorption, surface chemistry) properties. The framework material, surface chemistry and pore size must be carefully chosen to fit the intended use.

Although SiO_2 mesoporous materials are well studied and their preparation is straightforward, transition-metal oxide (TMO) mesoporous films are much more difficult to obtain, and only a limited amount of the different TMOs have been well studied. The TMO precursors show a high reactivity towards hydrolysis and condensation, requiring careful control during the sol–gel process in order to synchronize gelation and template ordering. This precise timing is required in an evaporation induced self assembly (EISA) process[5] to prepare well ordered mesoporous films. Moreover, transition metals tend to form discrete oxo-clusters instead of polymeric oligomers, which can only accommodate around the template micelles when condensation and hydrolysis are well controlled.[6–8]

Chemical and physical properties make zirconia an outstanding material in the palette of available TMOs: in contrast to SiO_2 derived films,[9] it withstands harsh alkaline, and oxidizing conditions; its affinity for phosphates like nerve agents and pesticides has already been exploited in the preparation of sensors[10] and can be used to tune the surface properties of the material.[11] It also has a very good thermal resistance and high refractive index, while its relatively high thermal expansion coefficient makes it also suitable for metal coating.[12] Zirconia-based mixed oxides are also crucial to strategic technologies, like yttria-stabilized zirconia (YSZ) in solid-oxide fuel cells and ceria–zirconia in catalysis. Moreover, unlike titania, zirconia is transparent in the UV region and does not photochemically degrade functionalizing agents attached to its surface.

In the last ten years, a few methods for the preparation of mesoporous zirconia thin films have been described. The first articles by Crepaldi *et al.* described the use of Pluronic F127 and Brij-58 as templates for the preparation of pure and substituted zirconia from $ZrCl_4$.[13,14] These first reports showed that a two-step procedure is needed in order to obtain homogeneous, optical quality films: the material is first cast on a disordered state, and a highly ordered mesopore structure is obtained only after exposing the freshly deposited film to water vapors. This treatment adds an additional processing step that needs to be controlled, and often leads to poor reproducibility in film characteristics, especially in the case of Brij-type templates. Later, non-commercially available KLE was used as a template, using THF as a cosolvent,[15] and a procedure using F127 as a

[a]*Escuela de Ciencia y Tecnología, Universidad Nacional de San Martín, Argentina*
[b]*Gerencia Química, Centro Atómico Constituyentes, Comisión Nacional de Energía Atómica, Av. Gral Paz 1499 (B1650KNA), Argentina. E-mail: zelcer@cnea.gov.ar; Fax: +54 6772 7886; Tel: +54 116772 7032*
[c]*DQIAyQF, FCEyN, Universidad de Buenos Aires, Argentina*

† Electronic supplementary information (ESI) available: GISAXS, XRR, DRIFT spectrum, FESEM images of samples treated at high temperatures, XRD pattern, FESEM images of bilayer films, transmission spectra and refractive indexes of films. See DOI: 10.1039/c2tc00319h

template followed by supercritical extraction was reported.[16] Most of the published methods rely on the use of highly acidic $ZrCl_4$ solutions, which are unsuitable for casting the films on sensitive substrates, like metals and some oxides such as FTO. Very recently a procedure using less acidic conditions was also reported, but material characterization was poorly performed and only one surfactant was studied.[17]

The combined use of low pH and complexing agents in order to control the sol–gel chemistry of metal oxide is well known. Nevertheless, this strategy has seldom been used for the preparation of ordered mesoporous materials. Boettcher *et al.* used acetate and trifluoroacetate together with acidic conditions to prepare different pure and mixed oxide mesoporous xerogels.[18] The bidentate complexant acetylacetonate was used in the preparation of titania sols for the preparation of mesoporous particles,[19] xerogels[20] and thin films,[21] and very recently for the preparation of Al_2O_3 films.[22] To the best of our knowledge, no reports on the use of acetylacetonate in the preparation of ZrO_2 ordered mesoporous thin films can be found in the literature.

In this paper a new, simple and reproducible one-step procedure is presented, that uses less acidic conditions than those previously reported and works with commercially available[23] surfactants, whether non-ionic, or cationic, such as CTAB. In contrast to many previously published methods, the film quality and pore ordering are not very sensitive to the relative humidity during deposition.

Experimental

Materials

Zirconium *n*-propoxide 70% in propanol, the ionic surfactant cetyltrimethylammonium bromide (CTAB) and triblock copolymers Pluronic® F127 ($M_w \sim 12\,600$) and P123 ($M_w \sim 5750$) were obtained from Aldrich. The complexant 2,3-pentanedione (acetylacetonate, acac), absolute ethanol, HCl (35%) and diblock copolymer Brij®58 ($C_{16}H_{33}(OCH_2CH_2)_{20}OH$, B58) were purchased from Merck. Water (resistivity 18 MΩ) was obtained from a Millipore® system. Glass slides were carefully cleaned and rinsed with acetone and pure water before using. Appropriate size silicon slides were cut from a wafer (Cemat Silicon S.A) and cleaned using the standard RCA SC-1 procedure.[24]

Sols preparation

Sols were prepared by mixing ethanol, acac, zirconium propoxide, HCl (35%), water and the surfactant in a molar ratio of $40 : 1 : 1 : 1 : 20 : x$, where x was 0.005 for F127, 0.05 for Brij58, 0.012 for P123 and was varied from 0.1 to 0.2 in the case of CTAB. First the acac, then alkoxide and finally the surfactant were added to 80% of the total amount of ethanol, and the mixture was stirred for a minute. Then HCl and water were dissolved in the remaining amount of ethanol and this mixture was added dropwise under stirring to the initial solution. The sols were stirred for one hour at room temperature before using. Sols without the surfactant were prepared to deposit dense films, and sols without HCl were also prepared to evaluate the influence of this reactant on sol stability and mesopore ordering.

Film production

Films were prepared by dip-coating the substrates in the sols, at withdrawing speeds ranging from 0.5 to 4.0 mm s^{-1} at controlled relative humidity (RH) of either 20% or 50% and room temperature (*ca.* 25 °C). The films were then transferred to chambers of controlled RH set at 50% for 24 h. A gradual thermal treatment was then applied, heating the films first for 24 h at 60 °C, then for 24 h at 130 °C and finally for 2 h either at 200 °C or 350 °C. Films were then briefly rinsed with water, then with ethanol and finally dried at 130 °C before performing any spectroscopic measurements. Some samples were further subjected to fast thermal treatments (15 minutes) up to 650 °C in order to assess the effect of higher temperatures on the porosity of the films. Bilayer films were deposited by using mesoporous films treated up to 200 °C as substrates. The films used for the alkaline resistance test were cast over dense ZrO_2 films prepared using sols without surfactant. Samples are named ZX, where X indicates the surfactant used for as a porogen: F for F127, B for Brij58, P for P123 and C for CTAB templated films.

Characterization

Films thickness and porosity were measured by X-ray reflectometry (XRR) at the XRD2 line of the Laboratorio Nacional de Luz Síncrotron (LNLS) at Campinas, Brasil, and by environmental ellipsoporosimetry (EP) using a Sopra GE-5A spectroscopic ellipsometer. The porosity was estimated from XRR data by measuring the change of the critical angle when the RH changed from 0% to over 90%. The degree of densification was estimated comparing the measured electronic density of the walls with that of the theoretical one of pure bulk zirconia.[25]

Film morphology, pore ordering and semiquantitative elemental analyses were performed by field emission scanning electron microscopy (FESEM) and energy-dispersive X-ray spectroscopy (EDS) using a SEM ZEISS LEO 982 GEMINI (CMA, FCEyN-UBA) equipped with an INCA X-Sight system (Oxford Instruments), operating at 5 kV for imaging and 20 kV for EDS. Pore ordering was also studied on samples deposited onto thin-glass by small angle X-ray scattering with 2D detection (SAXS) at the SAXS2 line of LNLS, and on thick-glass deposited samples by GISAXS at the XRD2 line.

Transmission electronic microscopy (TEM) was performed using a Philips CM200 operating at 180 kV (Gerencia de Materiales-CNEA). Samples were scratched off from the substrate and deposited on carbon-coated copper grids (EMS).

X-Ray diffraction was performed on a Panalytical Empyrean diffractometer using a 2θ scan at a fixed incidence angle of 0.240°, employing Cu Kα radiation.

Pore size distribution was estimated by EP. This technique relates the changes in thickness and refractive index of a porous film measured at different RH to the amount of adsorbed water in the pores. The pore size distribution is then derived from the amount of adsorbed water using standard porosimetry formalisms. Full details of this technique can be found elsewhere.[26]

Diffuse reflection Fourier-transform infrared spectroscopy (DRIFTS) was measured by Nicolet Magna-IR 560 with a

Spectroline DRIFTS accessory, using KBr as a support and a resolution of 4 cm^{-1}.

Results and discussion

Synthesis strategy

The mesoporous ZrO_2 thin films were prepared using a sol–gel based evaporation induced self assembly (EISA)[5] route. This approach requires careful tuning of the sol composition in order to (a) compatibilize the interactions between the surfactant and the inorganic polymer at the hybrid interface[27] and (b) adjust the polymerization and mesophase formation kinetics.[6] In order to achieve a highly ordered mesopore system through EISA, hydrophilic inorganic nanobuilding blocks with a low degree of condensation must be produced in the precursor solutions.[7,28] Usually, extremely high acid concentrations are used to prevent extensive condensation of transition metal oxides (TMOs).[29] Indeed, most published methods for preparing mesoporous ZrO_2 thin films rely on extremely low pH (HCl : Zr ratios from 2.4 to 4) to control the condensation kinetics.

Among the TMOs, sol–gel processing of zirconia-based materials usually requires carefully chosen conditions: the high difference between its preferential coordination number (6 and 7) and charge (4) leads to fast hydrolysis and condensation.[30] In this work, we used a combined synthesis design approach, employing both acac as a ligand and a moderately low pH as a way to control the Zr–O–Zr condensation. The use of acac for modulating the sol–gel reactivity of zirconium alkoxides is well documented. Acac acts as a bidentate ligand, occupying two coordination positions and neutralizing only one charge, decreasing the hydrolysis and condensation kinetics of Zr(IV). Depending on the hydrolysis conditions, small oxo or hydroxo clusters and polymeric sols can form.[31] These small flexible entities are necessary for a proper ordering of the inorganic framework during the EISA process. However, complexation can lead to acac-capped Zr–oxo *closo* clusters that are relatively hydrophobic. Thus, the synthesis design includes excess water and a controlled quantity of acid ($Zr : H_2O : HCl = 1 : 20 : 1$), in order to partially hydrolyze the surface of the Zr–oxo clusters, rendering them more hydrophilic (see Scheme 1). This procedure permits to keep both a low condensation rate and hydrophilic Zr–oxo clusters, while reducing the acidic contents of the precursor solution. The resulting sols are very stable and age more slowly than sols prepared using only acac. Indeed, acid-free sols turn deep orange within 24 hours and finally gel after a few days. Sols prepared with both one equivalent of acid and one equivalent of acac to Zr do not gel even after 6 months. In addition, these sols have excellent wetting properties, being possible to cast films on hydrophobic substrates like PMMA.

The homogeneity and optical quality of TMO mesoporous thin films depend critically on the deposition conditions. The withdrawal speed, external humidity and sol temperature and viscosity play a fundamental role in the EISA process.[5] In order to avoid the difficulties that arise when mesoporous ZrO_2 films are prepared from $ZrCl_4$,[13] it is necessary to slow down the hydrolysis and restrain extended condensation,[30] thus producing small soluble polymeric intermediates. These

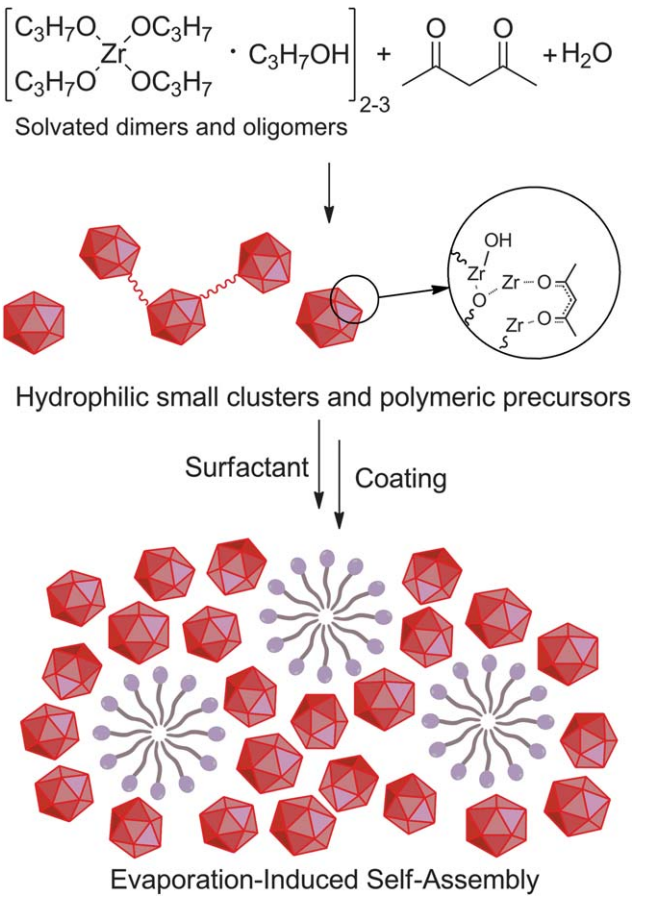

Scheme 1 Idealized formation of the ZrO_2-surfactant mesophase.

entities can accommodate around the forming micelles during the EISA process, yielding an ordered mesostructured material. The combination of low pH and a complexing agent results in a robust control, giving well ordered structures on samples deposited either at low (<20%) or moderate (50%) RH, showing that extensive hydrolysis–condensation is effectively inhibited.

Pore ordering

Transparent, optical-quality films with well ordered mesopores were obtained with all block copolymers tested. A direct observation of pore ordering can be achieved by TEM and FESEM. Fig. 1 shows TEM images of films templated with different surfactants after calcination at 350 °C. Large domains of ordered mesopores could be observed in all polymer templated samples. ZF and ZP films show interpore distances of *ca.* 16 nm with average pore diameters of 10 nm and 6 nm thick walls. ZB films show planes of pores separated by 7.8 nm, with 4 nm thick walls, while ZC films showed disordered pores, with approximately a 3 nm pore diameter and 3 nm wall thickness.

Pore arrays geometry of glass deposited samples was further evaluated using SAXS at normal and low-angle incidence (Fig. 2) and GISAXS (Fig. S1†). The observed pattern is compatible with a distorted $Im\bar{3}m$ cubic ordering for films prepared using both Pluronics® and Brij® templates. The interplanar distances are

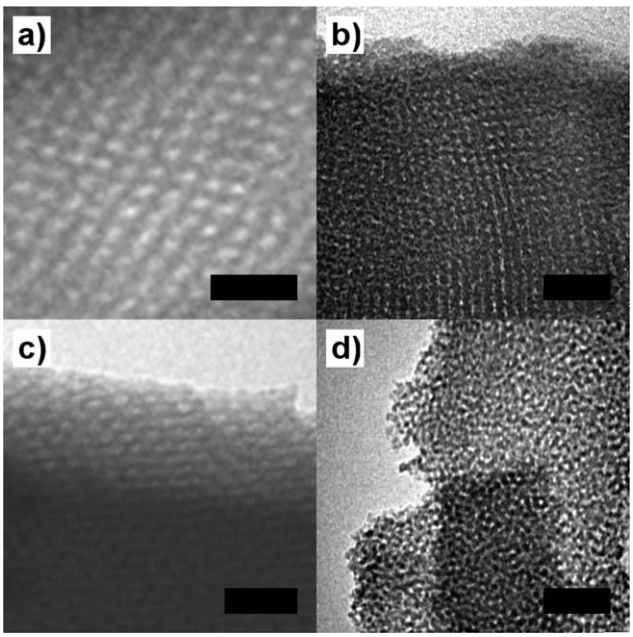

Fig. 1 TEM images of mesoporous ZrO_2 films prepared using (a) F127, (b) B58, (c) P123 and (d) CTAB as templates. Scale bars are 50 nm.

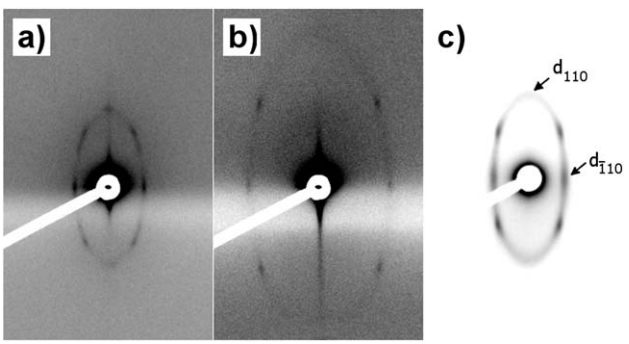

Fig. 2 SAXS patterns (3° incident angle) of films prepared using (a) F127, (b) B58 and (c) P123 as templating agents.

similar to those already found using these templating agents (Table 1). Experiments in transmission mode at incidence angles of 90° and 3° show that the samples are composed of polydomains in the *xy* plane oriented with the [110] direction parallel to the substrate.[32] A diffuse halo, compatible with a wormlike or short-range order was observed for ZC films (Fig. S1a†).

Despite the different molecular weights, the use of P123 and F127 resulted in similar interplanar distances. The same result has been observed in SiO_2/ZrO_2 mixed films, where increasing the Si : Zr ratio resulted in smaller interplanar distances.[33] Under these synthesis conditions hydrophilic zirconium oxo clusters are formed, which mix well with the PEO blocks of the surfactants. In this way the PEO blocks of both surfactants are pulled into the sol, leaving a PPO core of similar dimension in both cases. Indeed, ellipsoporosimetry shows that pore and neck sizes are quite similar for both surfactants (*vide infra*).

Table 1 Pore arrangement and distances as measured by SAXS for films cast at 50% RH

Surfactant	Structure	T/°C	d_{110}/nm	$d_{\bar{1}10}$/nm
F127	$Im\bar{3}m$	200	5.9	14.1
		350	3.6	14.1
B58	$Im\bar{3}m$	200	3.1	7.0
		350	1.9	7.0
P123	$Im\bar{3}m$	200	5.8	14.1
CTAB	Short-range	200		6.6[a]

[a] Characteristic distance.

The low angle diffraction patterns for samples deposited at 50% and 20% RH are similar, showing the same pore arrangement. Films cast at 20% RH showed slightly smaller interplanar distances than those cast at 50% RH, the difference being comparable to the error of the measurement: for ZF films the $\bar{1}00$ distance decreases from 141 Å to 138 Å.

Pore ordering at the films surface is further confirmed by FESEM images of film surfaces, where large-area domains of ordered pores are observed (see Fig. 3). Fourier transforms (FTs) of the images of polymer templated films show sets of discrete points confirming that the films are composed of large ordered domains. On the other hand, the FTs of ZC films show only a diffuse halo, characteristic of short-range order. The FT of the film prepared using B58 shows points corresponding to two different correlation distances: one pair of points situated at higher values in reciprocal space and two pairs at lower values. This typical "4 + 2" pattern is compatible with the [110] face of a $Im\bar{3}m$ cubic arrangement.[8]

A strong effect of the substrate was observed for P123 templated films, which exhibited only low-range order when deposited on silicon substrates and long range order when deposited on glass. As previously observed,[34] the nature of the substrate influences the ordering of the pores. Indeed, both SAXS and FESEM show that ZP films have a very good ordering when deposited on glass, but FESEM showed that a poor ordering is obtained when deposited on bare Si. A less dramatic, subtle effect is observed when the template is F127. Even if FESEM shows an excellent ordering of the pores also when deposited on Si, FTs of the images suggest that the exposed plane is not a [110] plane, as measured by SAXS. The FTs show points located at the vertices of a square. This kind of arrangement is compatible with the symmetry of the {100} planes of the proposed phase.[35]

Porosity and pore sizes

The films accessible porosity was determined using XRR. Measurements were carried out at high (>90%) and low (<1%) relative humidity, and the volume fraction of capillary condensed water filling the pores was calculated from the shift of the critical angle (for an example see Fig. S2†). The accessible porosities range from 17% for F127 up to 26% for ZC. The estimated framework density, taking into account the porosity calculated from water adsorption, is almost 80% of that of the

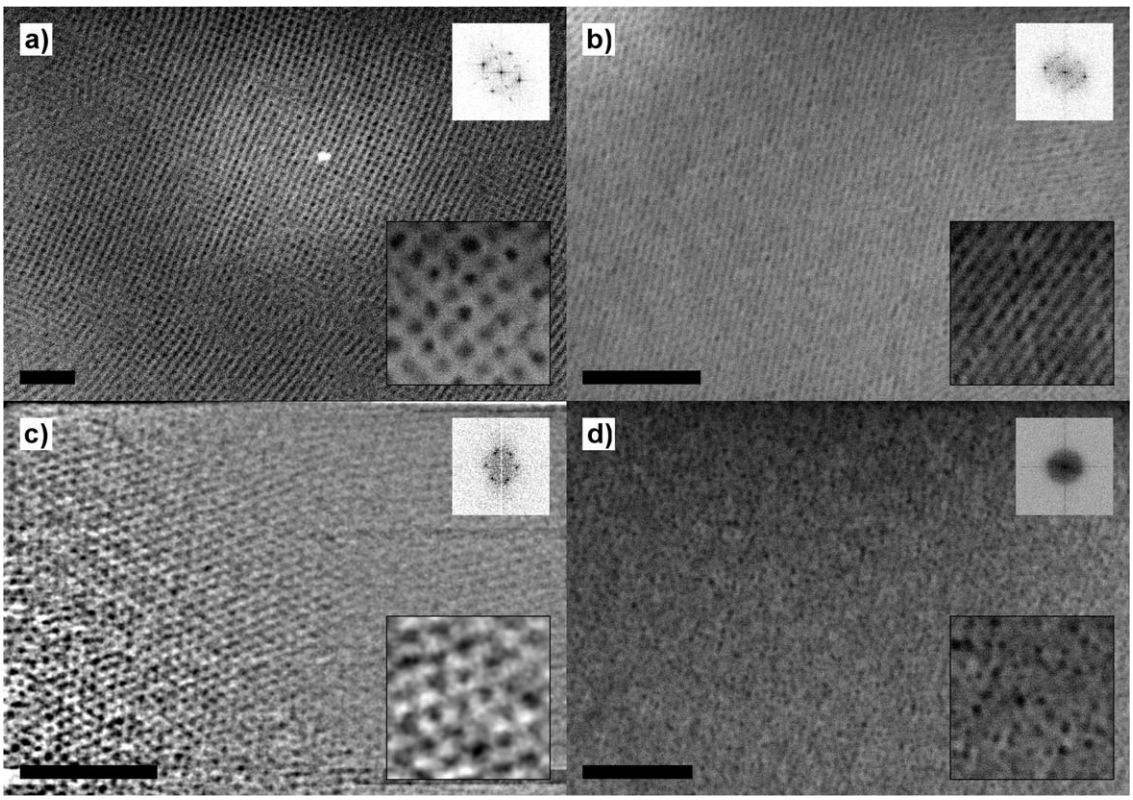

Fig. 3 FESEM images and selected area FTs of (a) ZF calcined at 200 °C, (b) ZB calcined at 350 °C, (c) ZP calcined at 200 °C and (d) ZC calcined at 200 °C. Scale bars correspond to 100 nm. All films were deposited on Si, except P123 that was deposited on glass (see text).

bulk cubic zirconia, showing a relatively high densification at 350 °C.

Pore size distributions (PSD), film thickness and porosity of thin films prepared with different templates were measured on samples heated at 350 °C by ellipsometric porosimetry using water as adsorbate[26] (Table 2). Typical adsorption–desorption isotherms with the corresponding PSDs are presented in Fig. 4. A strong hysteresis with type H2 loops[36] is observed between relative pressures 0.2 and 0.5 for Brij templated films and 0.4 and 0.85 for Pluronic templated films. Average pore and neck diameters are shown in Table 2. We find a good agreement in the porosity and thickness measurements from EP and XRR.

Film thickness can be controlled by varying the withdrawal speed. As determined by ellipsometry and XRR, the thickness can be varied from 40 nm up to 120 nm when the withdrawal speed goes from 0.5 mm to 4.0 mm s^{-1} (Fig. 5). The dependence of thickness with the withdrawal speed doesn't follow a power law as is usually postulated for dip-coating processes,[37] but the onset of a contribution from the capillary deposition regime[38] is observed at withdrawal speeds smaller than 2 mm s^{-1}. This behavior suggests that the viscosity of the sol has a great variation during the dip-coating process.

Table 2 Porosity and characteristic pore size of films

Surfactant	D^a/nm	Neck/nm	P^b (EPA)	P^b (XRR)
F127	6.9(2.5)	3.8(1.3)	15%	17%
B58	2.9(1.0)	2.1(0.6)	18%	22%
P123	6.2(2.5)	3.3(1.2)	27%	n/m
CTAB	5.6(2.2)	3.6(0.9)	23%	26%

[a] Pore diameter (deviation). [b] Porosity.

Thermal treatment

In order to improve the order and prevent the collapse of the mesostructure during heating, we followed a well established strategy of ageing and slowly heating of the films. The first treatment of 24 h at room temperature and 50% RH allows the surfactant to rearrange, improving the mesopore order in the final material.[13] The water content of the condensing films is determined by the interchange with the ambient. Thus RH must be kept high enough to prevent evaporation and condensation, keeping the dynamics in the gelled film fast enough, but not so high as to redissolve the material. The gradual thermal treatment that follows allows the material to condense slowly, producing a more robust material than a prolonged ageing followed by an abrupt calcination.[13]

Chemical evolution during thermal treatment was followed by DRIFTS on samples heated at 60, 130, 200 and 350 °C (Fig. S3†). All samples show a broad absorption below 700 cm^{-1}, indicating the formation of a Zr–O–Zr network. IR spectra of F127 templated films treated at 60 °C show several bands corresponding to the surfactant between 2900–2870 cm^{-1} and 1500–1250 cm^{-1}. A characteristic peak at 1534 cm^{-1} indicates

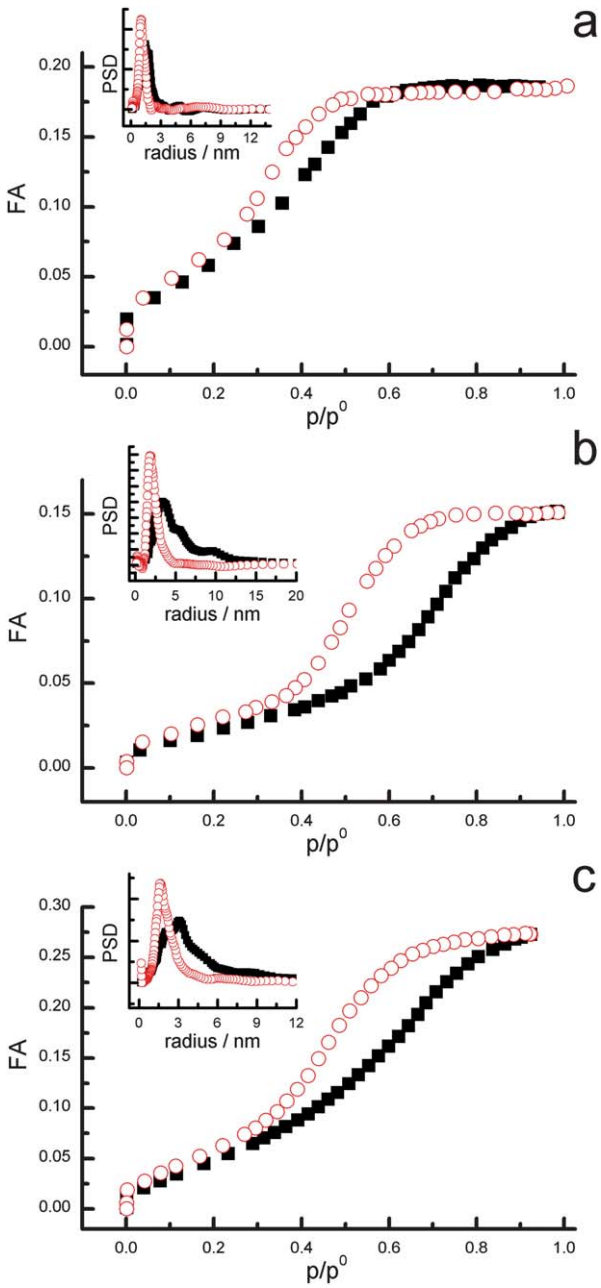

Fig. 4 Water adsorption–desorption isotherms and corresponding pore size distribution calculated for (a) ZB, (b) ZF and (c) ZP prepared at 1.0 mm s^{-1}. Closed boxes correspond to adsorption and open circles to desorption.

the presence of bidentate acac.[39] A strong adsorption is observed around 1590 cm^{-1}, probably resulting from the overlap between the bidentate species and adsorbed water. The absence of strong bands in the range 1650–1750 cm^{-1} shows that no free or monodentate acac remain in the film under these conditions. A strong band is observed around 1100 cm^{-1}, corresponding to C–C–O vibrations of the template. This band overlaps with the one corresponding to metal alkoxides (Zr–O–C), thus it is not possible to rule out that some alkoxide groups remain bonded. Nevertheless, due to the high excess of water employed ($H_2O/Zr = 20$) complete hydrolysis is expected.

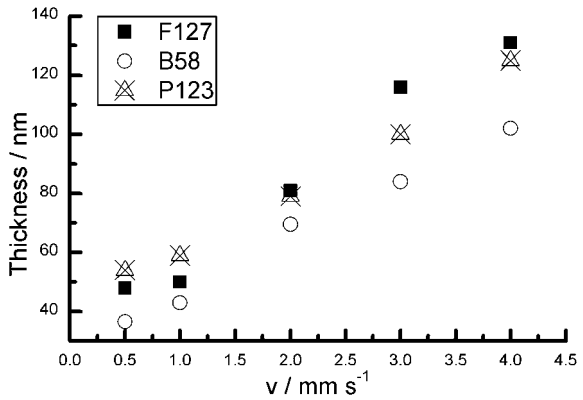

Fig. 5 Dependence of thickness with withdrawal speed for films deposited at 50% RH.

Interestingly, after treating at 130 °C the band corresponding to acac has almost disappeared, indicating that the complexing agent is largely eliminated even at this low temperature. At 200 °C the acac band has completely disappeared, and the 1100 cm^{-1} band and the bands corresponding to the surfactant are strongly weakened, indicating that the network is more developed and that the surfactant is partially decomposed at this temperature. At 350 °C these bands completely disappear, and only bands corresponding to adsorbed water or Zr–OH groups (3000, 1600 cm^{-1}), adsorbed carboxylates or carbonate (1353, 1381 cm^{-1}), and a strong wide band assigned to zirconyl groups (990 cm^{-1})[40] remain visible.

EDS analysis shows that the amount of residual chloride in films heated at 200 °C and 350 °C is below the detection limit of the technique (around 0.3% atom), see Fig. S4.† Interestingly, we found that rinsing of the films is crucial to remove debris that exudes from the film during thermal treatment. Indeed, if the films treated at 200 °C are not rinsed, the Cl to Zr ratio is 37%.

Heating contracts sol–gel derived films, distorting the $Im\bar{3}m$ pore structure. As the film is anchored to the substrate, the [$\bar{1}$10] interplanar distance does not change upon heating, while the [110] suffers heavy contraction. This uniaxial distortion of the cubic structure goes from ~57% in films heated at 200 °C to ~73% in films heated at 350 °C. The observed interplanar distances are shown in Table 1.

The effect of heating at higher temperatures was studied on P123 and F127 templated films supported on silicon. Samples were heated for 15 minutes at different temperatures up to 650 °C. Strong differences were observed depending on the surfactant used as a porogen. ZF films showed the same appearance under FESEM between 350 and 650 °C, while ZP films showed the gradual appearance of a grid-like structure, where adjacent pores join into a slit-like pore[41] (Fig. S5†). EP of high-temperature (500–650 °C) treated ZF (Fig. 6a) results in isotherms of similar shape for all, with an H2 hysteresis loop. This indicates that the pore morphology of these films is maintained. The total porosity increases with temperature up to 600 °C, and then decreases at higher temperatures. A similar behavior was observed in mesoporous TiO_2 films.[42] The initial increase of

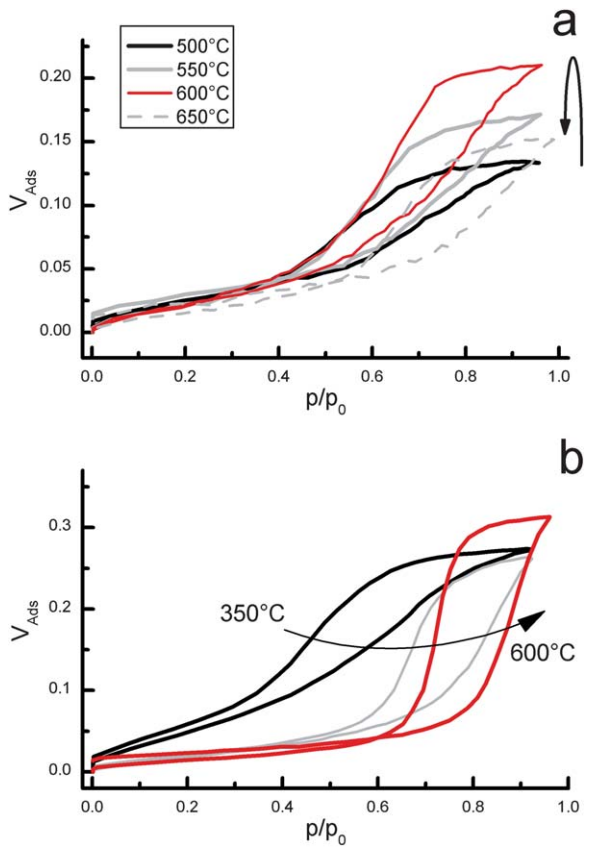

Fig. 6 Thermal evolution of the isotherms for (a) ZF films and (b) ZP films.

accessible porosity is attributed to a more complete decomposition of organic residues and better connectivity due to sintering, while the decrease at higher temperatures is attributed to extensive sintering. On the other hand, EP of ZP films show a shift of the hysteresis loop toward higher relative pressures (Fig. 6b), changing from the H2 to H1 type as the pores become slit-like. X-Ray diffraction studies performed on samples treated at 600 °C show that the mesoporous films have crystalline walls. Grazing incidence diffraction patterns present peaks compatible with tetragonal zirconia; the presence of a small amount of cubic zirconia can't be ruled out (Fig. S6†).

The different thermal behavior could be because of two reasons: (a) the different alignment of the pore array when using these surfactants hinders the morphological changes in the case of F127 and (b) since F127 has longer PEO blocks, films prepared using it as a template have a more discontinuous microstructure than those prepared using P123. When these films are subjected to a rapid heating, the discontinuities hinder the growth of nucleating crystals, minimizing the morphological changes due to crystallization and diffusive sintering.

Acidity and pore ordering

Changing the total concentration or the surfactant/metal ratio did not lead to ordered pores in the case of CTAB. Typical pore sizes of CTAB-templated mesoporous materials are around 2 nm, which is about the smallest expected size for the zirconium nanobuilding blocks (NBB) present in the solution: forced ageing experiments showed that using 1.1 equivalent of the complexing agent and 0.8 equivalents of acid, colloidal particles with a mean hydrodynamic diameter of 2–3 nm are obtained.[39] The same study showed that the particle size of the sol increases with water content, and with lower complexing ratios. After a critical water content ($H_2O : Zr = 10$), the particle size reaches a *plateau* at 10 nm and does not increase any longer. Thus, the mismatch between the NBB and micelle sizes prevents the micelles from ordering and produces a material where the characteristic distance is given by the combination of micelle and NBB sizes.

The addition of acid is necessary to stabilize the sol. Low pH inhibits extensive Zr(IV) condensation that will lead to precipitation. High acid concentration lowers the proportion of hydroxo-ions present. Furthermore, the clusters acquire a positive charge (for comparison, the IEP of ZrO_2 is between 4 and 11), thus stabilizing the sols. Besides acting as a condensation inhibitor, we found that the presence of acid is needed in order to obtain ordered mesopores: films prepared without the addition of acid under otherwise equivalent conditions did not show diffraction when examined with SAXS. The protonation of PEO segments of Pluronic and Brij surfactants could favour the formation of micelles, but it is not the only role played by acid. SAXS patterns of films prepared using the ionic surfactant CTAB as a template in the absence of acid do not show the diffracted halo associated with low-range order. In order to ensure a proper cooperative assembly of the ZrO_2 clusters and the templating agent, a compatible interface between both phases must exist.[43] At high proton concentration, the ZrO_2 surface is protonated, and $(S^0H^+)(X^-I^+)$ and hydrogen-bond mediated $(S^0)(I^0)$ hybrid interfaces[23] are developed.

Properties as a building block in multilayer devices

The availability of mesoporous zirconia thin films enables its use as a building block in complex structures, like distributed Bragg reflectors (DBRs)[3] or the preconcentration layer on selective electrodes.[10]

In order to build DBRs it is necessary to deposit successive layers of materials of different refractive indexes, building multilayer stacks. We studied the feasibility of employing the present method for building reflectors by casting a mesoporous SiO_2 layer on top of ZF and a ZF layer on top of mesoporous SiO_2. Cross-section FESEM images (Fig. S7†) show that the obtained bilayer films are even, and EP analysis shows that the porosity is well preserved in both films. Zirconia is a non-absorbing, high-refractive index optical material, which complements the palette of available mesoporous thin films that can be used to build photonic devices: mesoporous ZrO_2 thin films combine the UV-Vis transparency of SiO_2 with the high refractive index of TiO_2. Indeed, ZF films show a transmission of 84% (uncorrected for reflection losses) in the visible range, comparable to that of the bare substrate (Fig. S8†). In spite of the porosity, the films show a high refractive index. For all the templating agents used, the refractive index of films

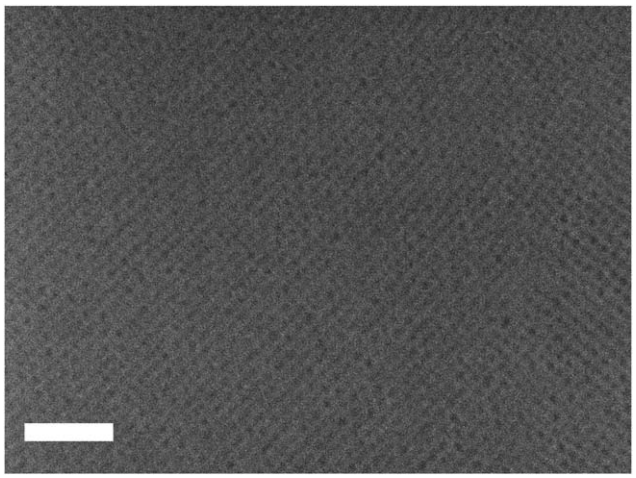

Fig. 7 FESEM image of a ZF film after being immersed for 18 h in 1 M NaOH solution. Scale bar is 100 nm.

treated at 350 °C goes from about 2 at 200 nm down to 1.6 at 900 nm (see Fig. S9†).

The mesoporous films prepared using the presented method are hard and do not scratch easily. Moreover the films withstand harsh alkaline conditions: the chemical stability of the films was tested by immersing ZF films in 1 M NaOH solutions for 18 h. FESEM images of the treated and untreated samples are indistinguishable (Fig. 7), and EP measurements show that the pore size distribution and porosity are unchanged. SAXS experiments indicate that the pore ordering is perfectly preserved, showing that the film can be used as protective or permselective layers of controlled porosity in devices that must work under extreme alkaline conditions.

Conclusions

In summary, we developed a very robust and straightforward one-step method for the deposition of optical quality mesoporous ZrO_2 thin films. The use of acid and acac as a complexing agent to control the hydrolysis and condensation rates of ZrO_2 results in stable sols and causes the deposition procedure to be insensitive to ambient humidity. The method results in well ordered, thermally stable mesoporous films with crystalline walls for a variety of PEO-based nonionic polymeric templates. Only very short-range ordering was observed when the small ionic surfactant CTAB was used as a template, probably because of a size mismatch between the ZrO_2 NBB and micelles. Our results show that the inclusion of acid does not only improve the stability of the sols but is necessary to obtain ordered mesoporosity in ZrO_2 films. These films withstand extreme chemical and thermal conditions, enabling their use as platforms for catalysts and optical or optoelectronic devices. The procedure can be easily extended to mixed metal systems of technical relevance like YSZ and zirconia–ceria oxides. In addition, the milder acidic conditions proposed here make this procedure suitable for building mesoporous Bragg reflectors on acid-sensitive materials such as transition metal oxides or polymers.

Acknowledgements

A. Wolosiuk, P.C. Angelomé, I.L. Violi and M.C. Fuertes are acknowledged for fruitful discussions and critical reading of the manuscript, and G. Zbihlei for the TEM images. V. Luca is acknowledged for DRX measurements. AZ and GJAASI are members of CONICET Scientific Staff. Financial support from grants PICT 34518 and 1848, UNSAM SJ10/20 and LNLS Scientific Project 5353 are acknowledged.

Notes and references

1 See *Chem. Mater.*, 2008, **20**(3), a special issue dedicated to Templated Materials.
2 A. Calvo, B. Yameen, F. J. Williams, G. J. A. A. Soler-Illia and O. Azzaroni, *J. Am. Chem. Soc.*, 2009, **131**, 10866; E. H. Otal, P. C. Angelomé, S. A. Bilmes and G. J. A. A. Soler-Illia, *Adv. Mater.*, 2006, **18**, 934.
3 S. Y. Choi, M. Mamak, G. von Freymann, N. Chopra and G. A. Ozin, *Nano Lett.*, 2006, **6**, 2456; M. C. Fuertes, F. J. López-Alcaraz, M. C. Marchi, H. E. Troiani, V. Luca, H. Míguez and G. J. A. A. Soler-Illia, *Adv. Funct. Mater.*, 2007, **17**, 1247.
4 C. Sanchez, C. Boissiere, D. Grosso, C. Laberty and L. Nicole, *Chem. Mater.*, 2008, **20**, 682.
5 C. J. Brinker, Y. Lu, A. Sellinger and H. Fan, *Adv. Mater.*, 1999, **11**, 579; D. Grosso, F. Cagnol, G. J. A. A. Soler-Illia, E. L. Crepaldi, H. Amenitsch, A. Brunet-Bruneau, A. Bourgeois and C. Sanchez, *Adv. Funct. Mater.*, 2004, **14**, 309.
6 G. J. A. A. Soler-Illia and P. Innocenzi, *Chem.–Eur. J.*, 2006, **12**, 4478.
7 G. J. A. A. Soler-Illia, E. Scolan, A. Louis, P.-A. Albouy and C. Sanchez, *New J. Chem.*, 2001, **25**, 156; G. J. A. A. Soler-Illia and C. Sanchez, *New J. Chem.*, 2000, **24**, 493.
8 G. J. A. A. Soler-Illia, P. C. Angelomé, M. C. Fuertes, D. Grosso and C. Boissiere, *Nanoscale*, 2012, **4**, 2549.
9 D. R. Dunphy, S. Singer, A. W. Cook, B. Smarsly, D. A. Doshi and C. J. Brinker, *Langmuir*, 2003, **19**, 10403; J. D. Bass, D. Grosso, C. Boissiere, E. Belamie, T. Coradin and C. Sanchez, *Chem. Mater.*, 2007, **19**, 4349.
10 G. Liu and Y. Lin, *Anal. Chem.*, 2005, **77**, 5894.
11 C. Queffélec, M. Petit, P. Janvier, D. A. Knight and B. Bujoli, *Chem. Rev.*, 2012, **112**, 3777.
12 K. Izumi, M. Murakami, T. Deguchi, A. Morita, N. Tohge and T. Minami, *J. Am. Ceram. Soc.*, 1989, **72**, 1465.
13 E. L. Crepaldi, G. J. A. A. Soler-Illia, D. Grosso and C. Sanchez, *New J. Chem.*, 2003, **27**, 9.
14 E. L. Crepaldi, G. J. A. A. Soler-Illia, A. Bouchara, D. Grosso, D. Durand and C. Sanchez, *Angew. Chem., Int. Ed.*, 2003, **42**, 347.
15 T. Brezesinski, M. Antonietti, M. Groenewolt, N. Pinna and B. Smarsly, *New J. Chem.*, 2005, **29**, 237; H. Fang, T. Wan, W. Shi and M. Zhang, *J. Non-Cryst. Solids*, 2007, **353**, 1657.
16 K. Wang, M. A. Morris, J. D. Holmes, J. Yu and R. Xu, *Microporous Mesoporous Mater.*, 2009, **117**, 161.

17 M. T. Soo, G. Kawamura, H. Muto, K. Y. Cheong, Z. Lockman, A. F. M. Noor and A. Matsuda, *J. Ceram. Soc. Jpn.*, 2011, **119**, 517.
18 J. Fan, S. W. Boettcher and G. D. Stucky, *Chem. Mater.*, 2006, **18**, 6391; S. W. Boettcher, M. H. Bartl, J. G. Hu and G. D. Stucky, *J. Am. Chem. Soc.*, 2005, **127**, 9721.
19 A. Beitollahi, A. H. H. Daie, L. Samie and M. M. Akbarnejad, *J. Alloys Compd.*, 2010, **490**, 311.
20 J. Zhang, Y. Deng, D. Gu, S. Wang, L. She, R. Che, Z.-S. Wang, B. Tu, S. Xie and D. Zhao, *Adv. Energy Mater.*, 2011, **1**, 241.
21 H.-S. Yun, K. Miyazawa, H. Zhou, I. Honma and M. Kuwabara, *Adv. Mater.*, 2001, **13**, 1377.
22 A. Mitra, D. Jana and G. De, *Microporous Mesoporous Mater.*, 2012, **158**, 187; A. Mitra, D. Jana and G. De, *Chem. Commun.*, 2012, **48**, 3333.
23 G. J. A. A. Soler-Illia, E. L. Crepaldi, D. Grosso and C. Sanchez, *Curr. Opin. Colloid Interface Sci.*, 2003, **8**, 109.
24 W. Kern and D. A. Puotinen, *RCA Rev.*, 1970, **31**, 187.
25 A. Gibaud and G. Vignaud, in *X-ray and Neutron Reflectivity: Principles and Applications*, ed. J. Daillant and A. Gibaud, Springer, Berlin Heidelberg, 2009, ch. 3, p. 94.
26 C. Boissiere, D. Grosso, S. Lepoutre, L. Nicole, A. Brunet-Bruneau and C. Sanchez, *Langmuir*, 2005, **21**, 12362.
27 C. Sanchez, G. J. A. A. Soler-Illia, F. Ribot and D. Grosso, *C. R. Chim.*, 2003, **6**, 1131.
28 G. J. A. A. Soler-Illia, C. Sanchez, B. Lebeau and J. Patarin, *Chem. Rev.*, 2002, **102**, 4093.
29 J.-P. Jolivet, in *Metal Oxide Chemistry and Synthesis*, John Wiley and Sons, 2000.
30 A. C. Pierre, in *Introduction to Sol–Gel Processing*, Kluwer Academic Publishers, 1998.
31 C. Sanchez, J. Livage, M. Henry and F. Babonneau, *J. Non-Cryst. Solids*, 1988, **100**, 65–76.
32 G. J. A. A. Soler-Illia, E. L. Crepaldi, D. Grosso, D. Durand and C. Sanchez, *Chem. Commun.*, 2002, 2298.
33 G. J. A. A. Soler-Illia, E. L. Crepaldi, D. Grosso and C. Sanchez, *J. Mater. Chem.*, 2004, **14**, 1879.
34 A. Chougnet, C. Heitz, E. Søndergard, J.-M. Berquier, P.-A. Albouy and M. Klotz, *J. Mater. Chem.*, 2005, **15**, 3340.
35 P. C. Angelomé, Ph.D. thesis, University of Buenos Aires, 2008.
36 S. Lowell, J. E. Shields, M. A. Thomas and M. Thommes, *Characterization of Porous Solids and Powders: Surface Area, Pore Size and Density*, Springer, 1st edn, 2004.
37 C. J. Brinker and G. W. Scherer, *Sol–Gel Science: The Physics and Chemistry of Sol–Gel Processing*, Academic Press Inc, San Diego, 1st edn, 1990.
38 M. Faustini, B. Louis, P.-A. Albouy, M. Kuemmel and D. Grosso, *J. Phys. Chem. C*, 2010, **114**, 7637.
39 M. Chatry, M. Henry, M. In, C. Sanchez and J. Livage, *J. Sol–Gel Sci. Technol.*, 1994, **1**, 233.
40 G. Socrates, *Infrared and Raman Characteristic Group Frequencies*, John Wiley and Sons, 3rd edn, 2004.
41 D. Grosso, G. J. A. A. Soler-Illia, E. L. Crepaldi, F. Cagnol, C. Sinturel, A. Bourgeois, A. Brunet-Bruneau, H. Amenitsch, P. A. Albouy and C. Sanchez, *Chem. Mater.*, 2003, **15**, 4562.
42 Y. Sakatani, D. Grosso, L. Nicole, C. Boissière, G. J. A. A. Soler-Illia and C. Sanchez, *J. Mater. Chem.*, 2006, **16**, 77.
43 Q. Huo, D. I. Margolese, U. Ciesla, D. G. Demuth, P. Feng, T. E. Gier, P. Sieger, A. Firouzi and B. F. Chmelka, *Chem. Mater.*, 1994, **6**, 1176.